Topographic Waves over the Continental Slope*

PING-TUNG SHAW

Institute of Oceanography, National Taiwan University, Taipei, Taiwan, R.O.C.

G. T. CSANADY**

Woods Hole Oceanographic Institution, Woods Hole, Massachusetts

(Manuscript received 24 March 1987, in final form 30 November 1987)

ABSTRACT

Current meter data taken during a one-year period over the continental slope and upper rise in three cross-isobath sections have been examined for energy distribution, coherence, and phase propagation of topographic waves. A peak at 15 days is present in the energy preserving spectrum of the near-bottom currents on the rise and slope. Phase propagation is offshore, and little energy is found in reflected waves. These results are consistent with earlier findings on the lower rise at Site D. Onshore energy flux associated with topographic waves is deflected by the continental slope, and wave energy propagates along isobaths on the lower slope and upper rise. The along-isobath coherence scale is about 200 km. The waves are probably generated by meanders in the Gulf Stream.

1. Introduction

In the late 1960s, long current meter records were collected at Site D (39°10'N; 70°00'W) over the continental rise south of Cape Cod and provided data for the study of low-frequency current fluctuations in the ocean. From those data, Thompson (1971) found significant vertical coherence at periods longer than 9 days between horizontal currents below 500 m. The phase varied little with depth, and the two horizontal velocity components from the same current meter were out of phase. Thompson suggested that the coherence was due to onshore propagating topographic waves generated by eddies in the Gulf Stream. Rhines (1971) noted that the energy spectrum in Thompson's paper was nearly depth-independent at periods between 9 days and a month, i.e., in the regime of linear topographic waves. He concluded that the observed barotropic structure was a strong indication of topographic waves. A later study at Site D by Thompson and Luyten (1976) revealed that coherence between temperature and the up-slope velocity, the vertical distribution of kinetic energy, and the frequency dependence of the principal axes at a single mooring site were all confirmed by Rhines' (1970) topographic wave model. They concluded that motion between 7 and 14 days was dominated by bottom-trapped topographic waves. The wavelength could not be calculated directly because data were obtained only at a single mooring site. Nevertheless, Rhines' (1970) model gave a wavelength between 90 and 160 km from the energy ratio at two depths.

Horizontal propagation of topographic waves on the continental rise was further studied by Thompson (1977). Data from an array of four current meter moorings allowed the direct calculation of the horizontal wavelength. He found that waves were transverse and phase propagation was offshore. Furthermore, the wavelength and frequency satisfied a dispersion relation of bottom-trapped topographic waves. The estimated horizontal wavelength was between 140 and 290 km at periods from 8 to 32 days, in agreement with earlier values from a single mooring. A more elaborate analysis of data from 15 moorings on the rise was made by Hogg (1981). The phases of velocity and temperature, described by empirical orthogonal functions, indicated propagation of plane topographic waves. Using a WKB model, Hogg could calculate ray paths and concluded that the waves were generated underneath the Gulf Stream. Other local studies on the rise include those of Hamilton (1984) off New Jersey, Kelley and Weatherly (1985) on the lower Scotian Rise, and Johns and Watts (1986) off Cape Hatteras.

The study of topographic waves was later extended to the continental slope. Ou and Beardsley (1980) ex-

* Woods Hole Oceanographic Institution Contribution No. 6523, Institute of Oceanography, National Taiwan University Contribution No. 283.

** Present affiliation: Department of Oceanography, Old Dominion University, Norfolk, VA 23508

Corresponding author address: Dr. Ping-Tung Shaw, Dept. of Marine, Earth and Atmospheric Sciences, North Carolina State University, Box 8208, Raleigh, NC 27695-8208.

amined the correlation between temperature and velocity fluctuations in a mooring section from the shelf to the slope south of Cape Cod. The results were compared with a baroclinic model of topographic waves over a steep bottom slope. Because the incident wave in their model extends to infinity in the along-isobath direction, significant wave reflection occurs. The latter conflicts with both Thompson's (1971) and later observations.

Topographic waves on the continental slope and upper rise were examined extensively by Louis et al. (1982). Clear distinct events of 21-day topographic waves, lasting for 3 or 4 cycles, were observed over the continental slope off Nova Scotia. Motion was barotropic at the slope–rise junction. The cross-isobath phase speed and wavelength calculated from phase differences could be explained by either a barotropic model or a baroclinic model. Therefore, density stratification is not important in their results. No reflected wave was observed as in the earlier studies at Site D.

These earlier studies have confirmed the existence of topographic waves on the continental rise and slope south of Cape Cod. However, two questions remain to be answered. First, what is the energy level of topographic waves on the slope? So far, only Louis et al. (1982) have examined topographic waves on the slope. Although they found 21-day energy at a depth of 230 m on the upper slope, the current meter is too shallow to be free from the baroclinic motion near the surface. It is interesting to note that the current at 690 m depth at the same site was very weak. An examination of the energy level will verify whether the slope is a good insulator for the transmission of wave energy as suggested by Csanady and Shaw (1983) and Shaw and Peng (1987). The other question is how wave energy propagates along isobaths. The array size in the experiments of Hogg (1981) and Louis et al. (1982) was too small to study the wave propagation in the along-isobath direction. Recent models of Louis and Smith (1982) and Shaw and Peng (1987) have shown that the lack of reflected waves on the rise in earlier observations is very probably due to the refraction of wave energy by topography. Current meter data from sites along isobaths are needed to verify the model results.

From 1983 to 1984, current meter moorings were deployed for one year on the continental slope along 71°W south of Cape Cod as part of the SEEP project. (For a brief description of SEEP moorings, see Churchill et al. 1986.) Additional data over the continental slope off New Jersey and off Chesapeake Bay are available from the MASAR experiments (Csanady and Hamilton 1988). Csanady et al. (1988) have presented statistics of near-bottom currents in these experiments. Time series from this dataset are analyzed in this paper. As in earlier studies, we will first calculate the autospectrum and the cross-spectrum to show the wave energy and cross-isobath propagation of the waves in the study region. However, the vertical structure of the waves cannot be determined because of the lack of vertical resolution in the data. The energy distribution and along-isobath coherence will then be examined for the wave refraction on the slope and rise. Possible source regions for topographic waves are suggested.

2. The data

The SEEP and MASAR arrays consist of three sections on the continental slope and upper rise (Fig. 1). The SEEP section is about 100 km to the west of Site D. The MASAR moorings are farther to the southwest. A cross-section of the SEEP current meters is shown in Fig. 2. Each current meter is identified by its mooring number followed by a sequential number beginning with the shallowest current meter in the mooring. The SEEP time series consist of two six-month pieces: the winter period from September 1983 to March 1984 and the summer period from April to October 1984. In summer, there are also data from MASAR moorings, although they only overlap partially with the SEEP series.

The raw velocity data were low-pass filtered with a 24-hour Gaussian filter. They were then subsampled once a day. The duration of the various time series

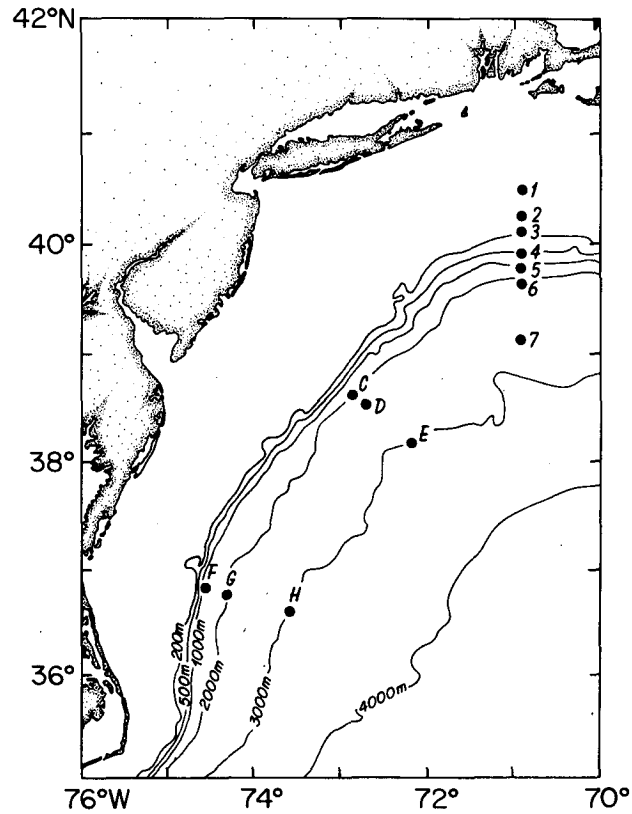

FIG. 1. Location of SEEP and MASAR moorings. Note that moorings D, G, and 3 are not used in this study because of bad data return or unsuitable current meter depth.

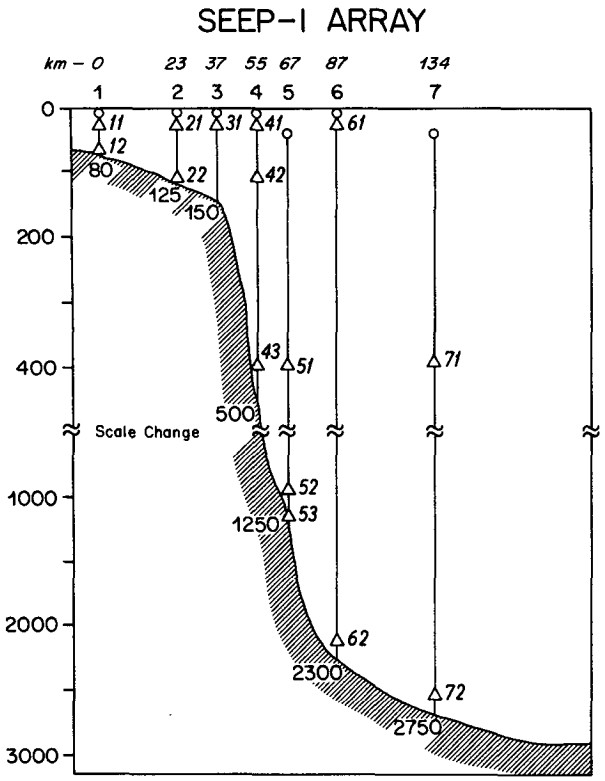

FIG. 2. Vertical section of SEEP moorings. Current meters are represented by triangles. Depth is in meters. Bottom depth is shown at each mooring site.

used in this study is listed in Table 1. A letter "W" or "S" is added to the current meter number of the SEEP time series to identify the winter or summer period. Wind stress from two weather buoys EB4 near Site E and EB8, 150 km east of the SEEP array, is also included. Because we are primarily interested in the barotropic or bottom intensified motion, current meters 100 m above the bottom in the deep water have been selected for analysis. This distance is above the bottom boundary layer and is also away from the region of strong baroclinic motion near the surface. On the shelf, current meters closest to the bottom have been used. Although bottom friction may be important here, the observed current represents a lower limit of the energy level on the shelf. Unfortunately, the bottom current meter on mooring 4 on the upper slope did not return data in either season, and there were no useful data from either bottom current meter on the shelf (moorings 1 or 2) in summer. Several mid-depth series from the SEEP array are included in Table 1 for comparison with the near-bottom series.

Fourier transformation was executed over 54-day segments of the time series in Table 1. The overlapping time is 27 days between two consecutive pieces. Auto- and cross-spectra were smoothed by a Hanning window and a band average over two adjacent frequencies. Further smoothing was obtained by ensemble averaging over all segments in each 6-month period. The resulting bandwidth is 0.77×10^{-3} cycle per hour (cph), and the lowest frequency band is centered at a period of 36 days (864 hours). There are 5 or 6 degrees of freedom in energy spectra, but only 4 in some coherence calculations between SEEP and MASAR moorings because of shorter overlapping time.

3. Wave spectra

In this section, energy level is described by energy preserving plots, in which the vertical axis is energy density times frequency. The area under the curve therefore represents the energy level in each frequency band. Energy spectra of selected time series are plotted in Fig. 3. There is little energy at periods shorter than a week over the slope and rise, i.e., in series 51W and 71W in Panel A and in all the series in panels B and C. The spectra are similar to those found in the earlier studies on the rise. Specifically, a peak at 15 days (370 hours) is present in most spectra. The period agrees with the 16-day peak found by Thompson (1977) at Site D. In comparison, spectra on the shelf or upper slope (12W, 22W and 42W in Panel A) have much higher energy at high frequencies. While high-frequency disturbances dominate in shallow water, energy is mostly in the low frequencies in the deep water.

The height of the peaks in the spectra shows both spatial and temporal variations. The energy level in the SEEP section is higher during the summer deployment (Panel C) than during winter (Panel B). In spite of the different energy levels at the two deployment periods, the peak in the spectrum on the slope (52W or 52S) is much smaller than the ones on the rise in the corresponding seasons (62W and 72W in winter or 62S and 72S in summer), indicating that little energy propagates onto the slope. A similar result was found by Louis et al. (1982). However, the MASAR data do not show such a decrease of energy toward the slope (Panel D). The lower energy level at Site E off Virginia than at sites 6 and H indicates that wave energy is not uniform along isobaths.

4. Current characteristics

The low-frequency energy shown in Fig. 3 can be decomposed into clockwise and anticlockwise components; the difference between the amplitudes of these two components is the rotary coefficient (Gonella 1972). It is zero when water particles move along a straight line; i.e., equal partition between the two components. This is the case in a plane transverse wave field. In the case of circular motion, the rotation of the current vector is either clockwise or anticlockwise and the magnitude of the rotary coefficient is unity. The rotary coefficient is used to describe the current characteristics.

Rotary coefficients of currents as a function of frequency are shown in Fig. 4. At 36 and 15 days, rotary

TABLE 1. Low-pass filtered time series.

Series	Latitude (N) (deg)	Latitude (N) (min)	Longitude (W) (deg)	Longitude (W) (min)	Depth (m)	Bottom (m)	Date From	Date To
12W	40	27.60	70	54.60	77	80	9-9-83	3-22-84
22W	40	15.00	70	55.20	120	124	9-10-83	3-22-84
42W	39	54.00	70	55.20	120	500	9-14-83	3-23-84
51W	39	48.00	70	54.00	400	1250	9-11-83	3-24-84
52W	39	48.00	70	54.00	1150	1250	9-11-83	3-24-84
62W	39	36.00	70	54.90	2201	2311	9-13-83	3-24-84
71W	39	7.80	70	54.60	400	2752	9-13-83	3-24-84
72W	39	7.80	70	54.60	2650	2752	9-13-83	3-24-84
41S	39	55.20	70	54.60	10	509	4-21-84	10-18-84
42S	39	55.20	70	54.60	120	509	4-21-84	10-18-84
51S	39	48.00	70	55.20	400	1277	4-22-84	10-18-84
52S	39	48.00	70	55.20	1150	1277	4-22-84	10-18-84
62S	39	36.00	70	55.80	2200	2366	4-22-84	10-19-84
71S	39	7.80	70	54.00	400	2752	4-23-84	10-19-84
72S	39	7.80	70	54.00	2650	2752	4-23-84	10-19-84
C4	38	35.00	72	55.30	1800	2000	3-1-84	9-6-84
E4	38	10.20	72	15.70	2900	3000	3-1-84	9-22-84
F9	36	51.60	74	34.10	905	1005	3-4-84	9-27-84
H2	36	32.70	73	30.80	2900	3000	3-5-84	9-28-84
EB4	38	18.00	71	42.00	—	—	9-11-83	3-30-84
EB8	40	9.00	69	24.00	—	—	4-25-84	10-15-84

coefficients of mid-depth and shallow currents (top panel) are generally different from zero. In contrast, rotary coefficients in the same lowest two frequency bands from near-bottom current meters (lower three panels) are less than 0.1, except at Site E. In the high frequency bands, the rotary coefficient is no longer small for either deep or shallow series. The smallness of the rotary coefficients indicates that low frequency near-bottom flow is due to plane topographic waves. Current at Site E is more complicated. The larger rotary coefficient at 36 days may be due to a superposition of plane waves or other motion.

Because flow is rectilinear, the direction of the major axis of the current ellipse at each site is well defined and is shown in Table 2 for periods at 36 and 15 days. It approximately parallels isobaths at all deep sites. Therefore, local wave vectors are nearly perpendicular to isobaths. A similar result has been obtained by Louis et al. (1982).

The coherence of currents at two depths is listed in Table 3. The component along the direction shown in Table 2 has been used. Significant vertical coherence has been found at the deep-water moorings at 36 and 15 days (e.g., between series 51 and 52 and between series 71 and 72). Phase differences are not significantly different from zero, suggesting coherent vertical motion on the lower slope and rise in agreement with the results of Thompson (1971) and Louis et al. (1982). Unfortunately, current meters 51 and 71 at 400 m are too shallow to determine if the wave is bottom trapped. The high energy level at 400 m at moorings 5 and 7 in Fig. 3 shows that baroclinic energy is present near the surface.

5. Cross-isobath wave propagation

To study the wave propagation, we have calculated the coherence and phase between currents from mooring pairs. Since the isobaths run approximately east–west in the SEEP array, the coherence between east velocity components was calculated. For MASAR moorings, the component along the direction shown in Table 2 was used. The coherence and phase difference were checked with the two-sided inner and outer cross-spectra between two velocity vectors (Mooers, 1973). The conclusions derived from the two methods are identical.

Significant coherence at low frequencies is found between most adjacent moorings in the deep water, and the phase increases offshore (current meters 52, 62 and 72 in Table 3). As an example, the coherence and phase between 62W and 72W are shown in Fig. 5. The coherence is significant at the 90% level in the lowest two bands. The phase difference is 90 degrees with the current at mooring 6 leading. Motion in the higher frequency bands is not coherent.

The phase relation is further studied using empirical orthogonal functions (EOFs) (Wallace and Dickinson 1972). In winter, the bottom series 22W, 52W, 62W and 72W are used. The mid-depth series 42W is also included to fill the gap on the upper slope. Since baroclinic energy has been found at 400 m at sites 5 and 7 in section 4, energy at current meter 42, which is 120 m deep, may not represent the topographic wave energy below the thermocline. One should be cautious in the interpretation of the results. In summer there are no data from the bottom current meters on the shelf and the calculation is limited to the deep water stations.

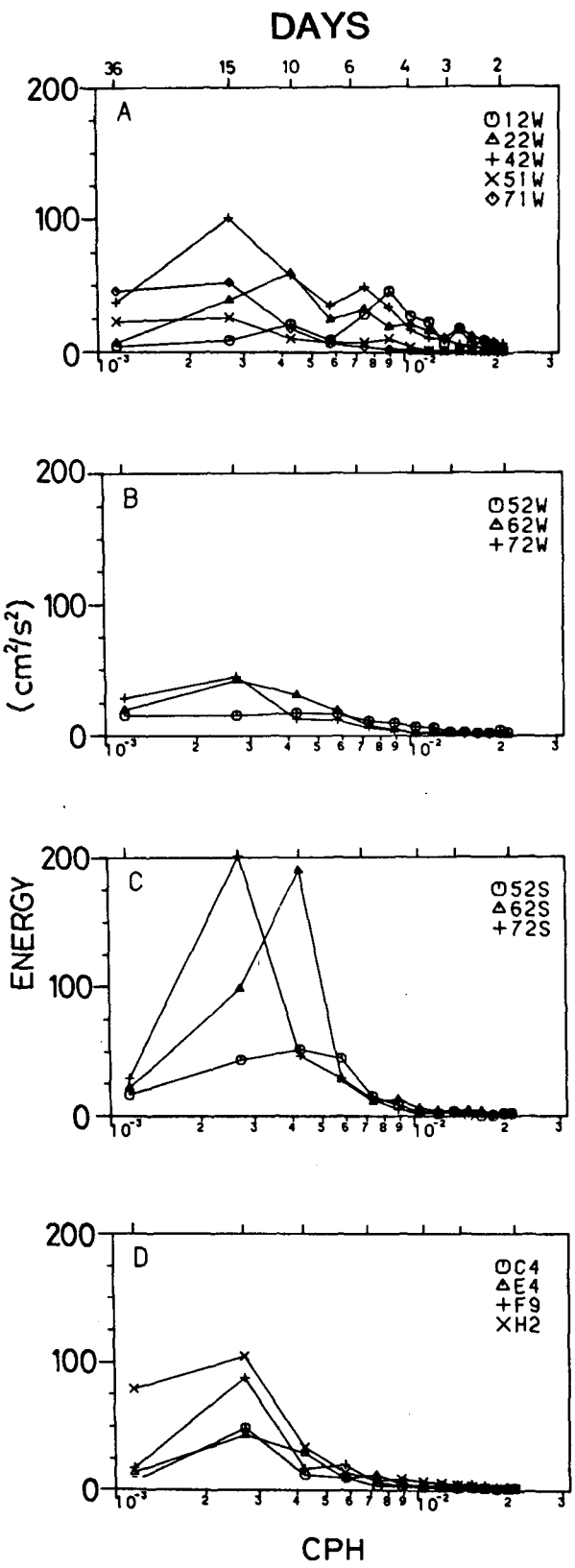

FIG. 3. Energy preserving spectra from selected series. Frequency is in cycles per hours (cph) and period is in days.

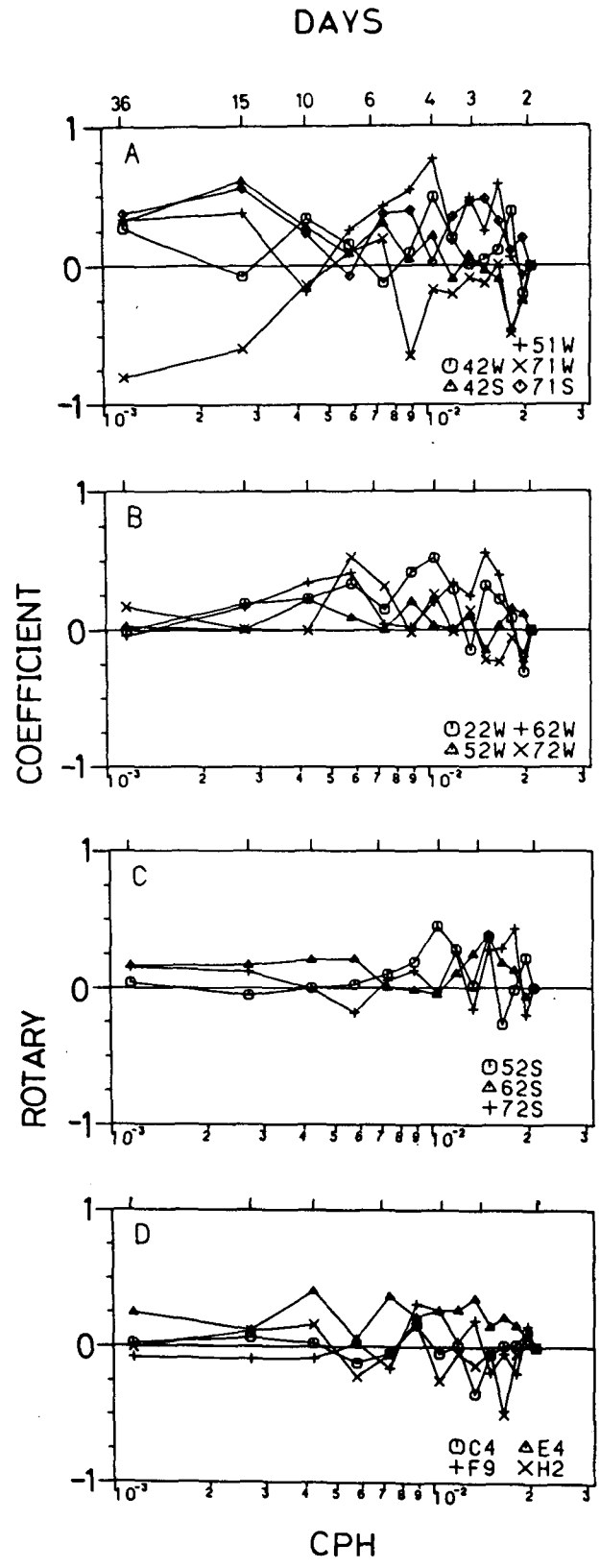

FIG. 4. Rotary coefficient as a function of frequency from selected time series. Horizontal axes are the same as in Fig. 3.

TABLE 2. Ellipse orientation of bottom current at 36 and 15 days in degrees clockwise from north.

	36 days		15 days	
Current meter	Winter	Summer	Winter	Summer
12	78	—	84	—
22	72	—	75	—
52	90	92	88	93
62	79	77	84	81
72	97	100	102	103
C4	—	50	—	51
E4	—	75	—	(115)
F9	—	15	—	16
H2	—	24	—	(52)

—: No data available.
Numbers in parentheses indicate ellipse stability lower than the 90% significance level.

Most variance of currents in the SEEP array can be explained by the first empirical orthogonal mode. Variance explained by the first two modes and coherence of currents with the first mode are listed in Table 4. Bottom currents are well correlated with the first mode at both 36 and 15 days in the deep water.

At 15 days, the first mode describes a wave whose amplitude decreases rapidly from mooring 7 on the rise to mooring 4 on the upper slope in summer (Fig. 6). The decrease in amplitude suggests that little energy reaches the upper slope. In winter some energy is present on the shelf, but the small amplitude at site 5 suggests that waves in the deep water and on the shelf are not related. The small amplitude on the lower slope is consistent with the smaller peak in the energy spectrum on slope in Fig. 3. Phase propagation associated with the first mode is offshore (Fig. 6). The phase difference between two moorings agrees with that in Table 3.

At 36 days the wave amplitude is very small on the shelf, but it is nearly constant from the rise to the upper slope (Fig. 7). Only in winter is a small minimum in amplitude present at site 5. The ratio of wave amplitude on the slope to that on the rise is higher at 36 days than at 15 days, but it is possibly due to the low energy level on the rise at 36 days. The high energy at current meter 42 may be due to the baroclinic motion, as mentioned earlier. The phase of the first mode again decreases onshore in both seasons. The slope of the curve increases slightly toward the continental slope, indicating shorter cross-isobath wavelengths on the slope.

The cross-isobath phase propagation agrees with earlier studies. Taking the direction perpendicular to the major axis shown in Table 2 as that of the wave vector at each site, we can calculate the local wavelengths from phase differences between two SEEP moorings. They are generally between 80 and 220 km at 15 and 36 days. These values are in the range found earlier (e.g., Hogg 1981; Louis et al. 1982).

Because there are only two stations in either MASAR section, the direction of offshore phase propagation cannot be determined. However, significant coherence is found between sites F and H (Table 3), indicating wave propagation. Motion is out of phase at 15 days. The phase difference is close to the one in the SEEP array. No coherence is found between currents at sites E and C at either 36 or 15 days (Table 3); there is no cross-isobath phase propagation at Site E.

TABLE 3. Coherence and phase between currents in the same cross-isobath section.

		36 days		15 days	
Between	Degrees of freedom	Coherence	Phase (deg)	Coherence	Phase (deg)
52W–62W	6	0.74	−58 ± 32	—	—
52S–62S	5	0.75	−63 ± 36	0.83	−80 ± 27
62W–72W	6	0.65	−78 ± 42	0.64	−108 ± 44
62S–72S	5	—	—	*	*
C4–E4	4	—	—	—	—
F9–H2	4	—	—	0.80	−173 ± 36
51W–52W	6	0.68	4 ± 38	—	—
51S–52S	5	0.78	24 ± 32	0.82	28 ± 28
71W–72W	6	0.64	−45 ± 43	0.65	−27 ± 42
71S–72S	5	—	—	0.89	7 ± 25
12W–22W	6	—	—	0.72	−29 ± 34
22W–42W	6	—	—	0.62	−142 ± 47
42W–51W	6	0.67	−64 ± 40	—	—
42S–51S	5	—	—	—	—
42W–52W	6	—	—	—	—
42S–52S	5	—	—	—	—

Note: a positive phase means the second series leading.
—: coherence lower than the 90% significance level.
*: marginal coherence at 85%.

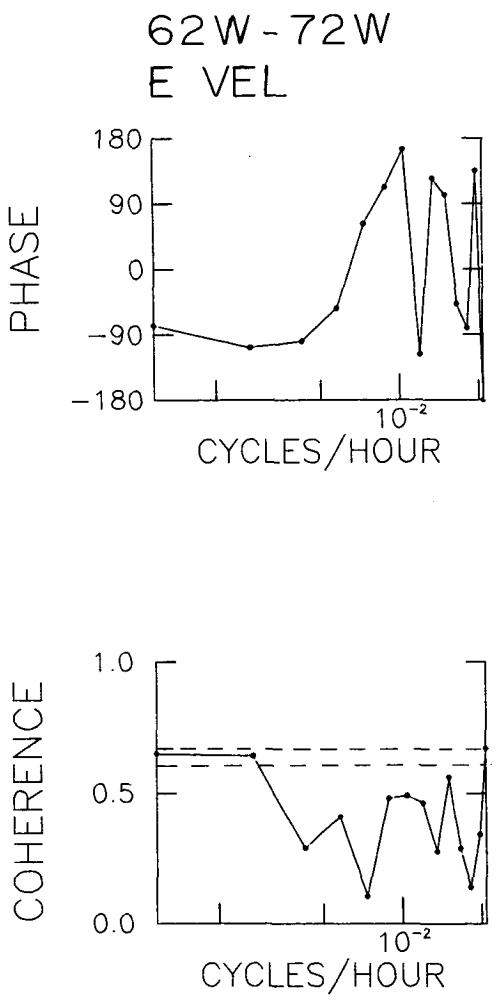

FIG. 5. Coherence and phase between the east components of velocity of 62W and 72W. The two dashed lines are confidence levels at 90 and 95%.

6. Along-isobath wave propagation

Significant coherence is found between currents at the SEEP sites and at Site C as well as between those at Site C and at sites F and H (Table 5). It is not surprising that current at Site E is not coherent with currents at any other sites. Therefore, there is wave propagation along isobaths on the slope and rise, but not to Site E. Phase differences are similar at 15 and 36 days (Table 5). The phase at Site C on the slope lags those at sites 5 and 6, but leads the phase at Site 7 on the rise. Therefore, lines of constant phase at SEEP turn clockwise relative to isobaths at both 15 and 36 days (see Fig. 1 for the direction of isobaths). This direction agrees with the major axes of current ellipses in Table 2. The phase velocity, which is perpendicular to the constant phase lines, has a small component to the west along isobaths, in agreement with the topographic wave theory.

The phase difference between MASAR sites C and F on the slope is not significantly different from zero (Table 5). The EOF analysis (not shown), using data from the three sites C, F and H has confirmed the phase differences. Therefore, constant phase lines are nearly parallel to isobaths on the slope. The phase velocity of topographic waves off Virginia is in a direction nearly perpendicular to isobaths.

7. Discussion

Although the characteristics of the waves at SEEP are similar to those at Site D, any comparisons with the models are not straight forward. The bottom slope at sites 6 and 7 is between 0.01 and 0.05, i.e., is one order of magnitude steeper than that at Site D. In addition, the large cross-isobath wavelength compared with the topographic scale makes the WKB approximation not appropriate. Recently Shaw and Peng (1987) used a numerical model to demonstrate the onshore propagation of topographic wave energy over realistic topography without the use of WKB approximation. They calculated the kinetic energy density distribution for topographic waves emitted from a point source at various frequencies. Although the strength of the source of topographic waves and the frictional coefficient in the ocean are not known, a qualitative comparison between the model and the observations is possible.

Topographic waves on the continental rise have periods longer than a week (e.g., Rhines 1970). Shaw and Peng (1987) have shown that sources on the continental rise are very effective in generating 36- and 15-day waves, but ineffective in generating 4-day waves.

TABLE 4. Percentage of variance explained by EOFs and coherence with the first mode for bottom current at SEEP.

Period (days)	Season	Degrees of freedom	Mode 1 (%)	Mode 2 (%)	Coherence with the first mode				
					22	42	52	62	72
36	winter	6	58	21	—	.69	.79	.88	.79
36	summer	5	58	22	*	.69	.87	.81	.74
15	winter	6	50	30	.70	.75	—	.75	.74
15	summer	5	74	18	*	—	.85	.83	.95

*: No data.
—: coherence insignificant at 90%.

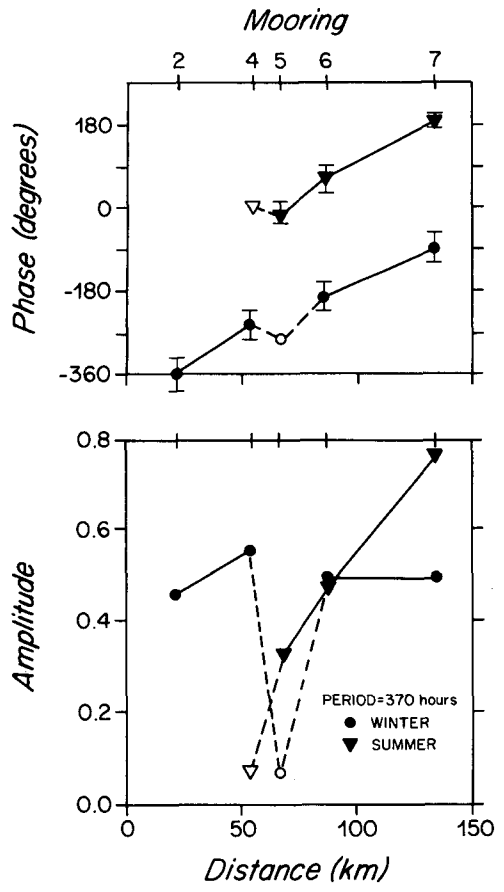

FIG. 6. Phase and amplitude of the first EOF at 15 days as a function of offshore distance in the SEEP section. Open symbols indicate that coherence is not significant at 90%.

Also, little low-frequency energy on the rise penetrates the slope. On the other hand, topographic waves generated by sources at 4 days on the shelf are coastally trapped. This is exactly what the observations have shown. We have found that the peak at 15 days in the energy spectra of SEEP series in section 3 is much higher on the rise than on the slope. The EOF analysis in section 5 also shows that the amplitude of the 15-day waves is very small at mooring 5. Therefore, the insulating effect of a steep continental slope (Csanady and Shaw 1983) should hold for topographic waves.

In the model of Shaw and Peng (1987), wave energy generated by a source on the upper rise propagates toward the slope and turns toward the direction of isobaths at the slope–rise junction (their Fig. 4). Results from the previous sections show that deep currents in the SEEP array are coherent, suggesting a common origin of the waves. Also there is little reflected wave energy, as shown by the small rotary coefficient and offshore increase in phase. Wave refraction is suggested by the coherence between currents at Site C and at the SEEP sites and the decrease in energy level from 7 to C. One concludes that the SEEP waves originate from a source to the southeast in the region where bottom-trapped topographic waves have been found by other authors. The low-frequency waves at SEEP are most likely a manifestation of the same bottom-trapped topographic waves.

Since energy at Site F is much higher than that at Site C, waves at F can not originate from the SEEP array. The lack of coherence at Site E with currents at other MASAR or SEEP moorings also shows that waves southwest of Site C are generated elsewhere. The model of Shaw and Peng (1987) shows that energy of topographic waves generated by a source on the slope propagates from Site C to F. It is legitimate to infer that waves at F and H are from sources close to the slope south of section C–E.

The onshore energy flux at the SEEP array suggests an offshore source. The waves are not driven by wind. (The result has been confirmed by the insignificant coherence between deep currents and wind at weather buoys EB4 and EB8.) Possible sources of the topographic waves include Gulf Stream rings and meanders. Louis and Smith (1982) suggested that a warm-core ring was the source of the 21-day oscillation off Nova Scotia. In the SEEP experiment, the only time when a warm-core ring was nearby was during October, 1983

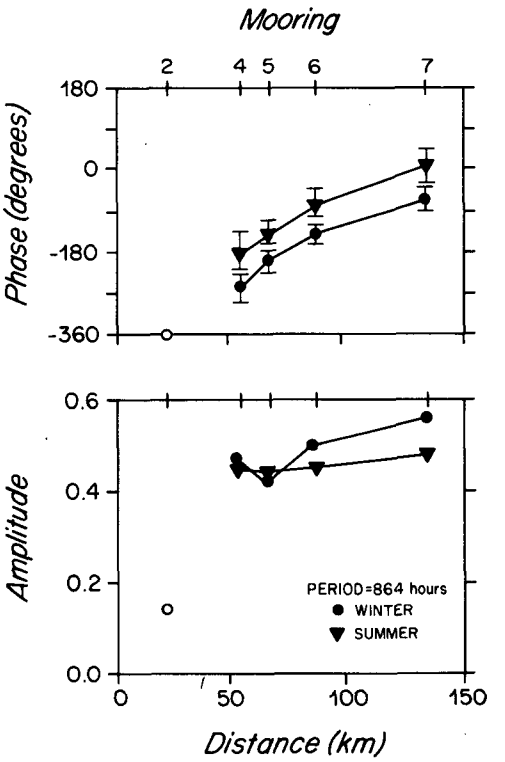

FIG. 7. Same as Fig. 6, but at 36 days.

TABLE 5. Coherence and phase between currents from different sections.

Between	Degrees of freedom	36 days		15 days	
		Coherence	Phase (deg)	Coherence	Phase (deg)
52S–C4	4	0.79	−122 ± 38	—	—
62S–C4	4	0.75	−37 ± 44	—	—
72S–C4	4	0.82	28 ± 34	0.95	19 ± 15
52S–E4	4	—	—	—	—
62S–E4	4	—	—	—	—
72S–E4	4	—	—	—	—
C4–F9	4	0.89	12 ± 24	0.86	−19 ± 28
C4–H2	4	—	—	0.75	178 ± 44
E4–F9	4	—	—	—	—
E4–H2	4	—	—	—	—

Note: a positive phase means the second series leading.
— : coherence lower than the 90% significance level.

(Churchill et al. 1986), but topographic waves were not observed at that time (Csanady et al. 1988). It is possible that topographic waves are excited at the SEEP and MASAR sites when the Gulf Stream meanders onto the rise and slope. Csanady (1988) has proposed that pressure torque on the interface during meandering of the Gulf Stream may generate topographic waves over a sloping bottom. This mechanism would be expected to be most intensive where meander amplitude peaks, i.e., 100 km or so east and west of the SEEP array (Halliwell and Mooers 1983; Cornillon 1986). The peak to the east may be related to the waves observed at the SEEP array, and the one to the west may have generated the waves in the MASAR array.

8. Conclusion

We have found that low-frequency topographic waves dominate the near-bottom motion on the continental slope and upper rise off the Mid-Atlantic Bight. Energy of these waves is mostly in periods longer than about a week. The continental slope effectively blocks up-slope energy transmission, and wave refraction occurs at the slope–rise junction. Waves are coherent to a distance of 200 km along isobaths from the SEEP array, and presumably come from Gulf Stream meanders 100 km or so farther southeast. Waves at MASAR moorings propagate along isobaths on the lower slope, and are probably generated by Gulf Stream meanders close to the slope between the two MASAR sections.

Acknowledgments. We would like to thank J. H. Churchill for his help during the data processing and Mr. C.-Y. Peng for drafting. The data were analyzed mostly at the Woods Hole Oceanographic Institution during a three month visit of PTS, supported by U.S. Department of Energy Contract No. DE-AC02-79EV10005. The writing of this paper was supported by the National Science Council of the Republic of China under Grant NSC75-0209-M002a-10.

REFERENCES

Churchill, J. H., P. C. Cornillon and G. W. Milkowski, 1986: A cyclonic eddy and shelf-slope water exchange associated with a Gulf Stream warm-core ring. *J. Geophys. Res.*, **91**, 9615–9623.

Cornillon, P., 1986: The effect of the New England Seamounts on Gulf Stream meandering as observed from satellite IR imagery. *J. Phys. Oceanogr.*, **16**, 386–389.

Csanady, G. T., 1988: Radiation of topographic waves from Gulf Stream meanders. Special SEEP issue, *Cont. Shelf Res.*, in press.

——, and P. T. Shaw, 1983: The "insulating" effect of a steep continental slope. *J. Geophys. Res.*, **88**, 7519–7524.

——, and P. Hamilton, 1988: Circulation of slopewater. Special SEEP issue, *Cont. Shelf Res.*, in press.

——, J. H. Churchill and B. Butman, 1988: Near-bottom currents over the continental slope in the Mid-Atlantic Bight. Special SEEP issue, *Cont. Shelf Res.*, in press.

Gonella, J., 1972: A rotary-component method for analyzing meteorological and oceanographic vector time series. *Deep-Sea Res.*, **19**, 833–846.

Halliwell, Jr., G. R., and C. N. K. Mooers, 1983: Meanders of the Gulf Stream downstream from Cape Hatteras 1975–1978. *J. Phys. Oceanogr.*, **13**, 1275–1292.

Hamilton, P., 1984: Topographic and inertial waves on the continental rise of the Mid-Atlantic Bight. *J. Geophys. Res.*, **89**, 695–710.

Hogg, N., 1981: Topographic waves along 70°W on the continental rise. *J. Mar. Res.*, **39**, 627–649.

Johns, W. E., and D. R. Watts, 1986: Time scales and structure of topographic Rossby waves and meanders in the deep Gulf Stream. *J. Mar. Res.*, **44**, 267–290.

Kelley, E. A., and G. L. Weatherly, 1985: Abyssal eddies near the Gulf Stream. *J. Geophys. Res.*, **90**, 3151–3159.

Louis, J., and P. C. Smith, 1982: The development of the barotropic radiation field of an eddy over a slope. *J. Phys. Oceanogr.*, **12**, 56–73.

——, B. Petrie and P. Smith, 1982: Observations of topographic Rossby waves on the continental margin off Nova Scotia. *J. Phys. Oceanogr.*, **12,** 47–55.

Mooers, C. N. K., 1973: A technique for the cross spectrum analysis of pairs of complex-valued time series, with emphasis on properties of polarized components and rotational invariants. *Deep-Sea Res.*, **20,** 1129–1141.

Ou, H. W., and R. C. Beardsley, 1980: On the propagation of free topographic Rossby waves near continental margins. Part 2: Numerical model. *J. Phys. Oceanogr.*, **10,** 1323–1339.

Rhines, P. B., 1970: Edge-, bottom-, and Rossby waves in a rotating stratified fluid. *Geophys. Fluid Dyn.*, **1,** 273–302.

——, 1971: A note on long-period motions at site D. *Deep-Sea Res.*, **18,** 21–26.

Shaw, P. T., and C. Y. Peng, 1987: A numerical study of the propagation of topographic Rossby waves. *J. Phys. Oceanogr.*, **17,** 358–366.

Thompson, R. O. R. Y., 1971: Topographic Rossby waves at a site north of the Gulf Stream. *Deep-Sea Res.*, **18,** 1–20.

——, 1977: Observations of Rossby waves near site D. *Progress in Oceanography,* Vol. 7, Pergamon, 135–162.

——, and J. Luyten, 1976: Evidence for bottom trapped topographic Rossby waves from single moorings. *Deep-Sea Res.*, **23,** 629–635.

Wallace, J. M., and R. E. Dickinson, 1972: Empirical orthogonal representation of time series in the frequency domain. Part I: Theoretical considerations. *J. Appl. Meteor.*, **11,** 887–892.